

# Dynamical and chemical characteristics of tropospheric intrusions observed during START08

Cameron R. Homeyer,<sup>1</sup> Kenneth P. Bowman,<sup>1</sup> Laura L. Pan,<sup>2</sup> Elliot L. Atlas,<sup>3</sup> Ru-Shan Gao,<sup>4</sup> and Teresa L. Campos<sup>2</sup>

Received 21 September 2010; revised 1 December 2010; accepted 30 December 2010; published 24 March 2011.

[1] Intrusions of air from the tropical upper troposphere into the extratropical stratosphere above the subtropical jet potentially have a significant impact on the composition of the lowermost stratosphere (the stratospheric part of the “middle world”). We present an analysis of tropospheric intrusion events observed during the Stratosphere-Troposphere Analyses of Regional Transport 2008 (START08) experiment using kinematic and chemical diagnostics. The transport processes operating during each event are discussed using high-resolution model analyses and backward trajectory calculations. Each intrusion observed during START08 can be related to a Rossby wavebreaking event over the Pacific Ocean. Trajectory analysis shows that the intruding air masses can be traced back to the tropical upper troposphere and lower stratosphere. In situ chemical observations of the tropospheric intrusions are used to estimate the mixing time scales of the observed intrusions through use of a simple box model and trace species with different photochemical lifetimes. We estimate that the time scale for an intrusion to mix with the background stratospheric air is 5 to 6 days. Detailed analysis of small-scale features with tropospheric characteristics observed in the stratosphere suggests frequent irreversible transport associated with tropospheric intrusions. Trace gas distributions and correlations are consistent with the dynamics of the high-resolution NCEP GFS analyses, suggesting that these features are captured by the GFS assimilation and forecast system. A global analysis of intrusion events observed during the START08 time period (April–June 2008) is also given.

**Citation:** Homeyer, C. R., K. P. Bowman, L. L. Pan, E. L. Atlas, R.-S. Gao, and T. L. Campos (2011), Dynamical and chemical characteristics of tropospheric intrusions observed during START08, *J. Geophys. Res.*, 116, D06111, doi:10.1029/2010JD015098.

## 1. Introduction

[2] The mechanisms of stratosphere-troposphere exchange (STE) continue to be an area of active research. The influence of STE on the composition of the upper troposphere and lower stratosphere (UTLS), particularly in the “middle world” [Hoskins, 1991], has important consequences for chemistry, climate and the radiation budget. As outlined by Holton *et al.* [1995] and Stohl *et al.* [2003], STE is not fully understood due to the existence of multiple transport pathways in the UTLS and the irregular occurrence of many exchange events.

[3] STE can occur in both directions: stratosphere-to-troposphere transport (STT) and troposphere-to-stratosphere transport (TST). Stratospheric intrusions (tropopause folds) are an important STT mechanism, and have been the focus of many research studies and aircraft experiments [e.g., Danielsen, 1968; Shapiro, 1980; Browell *et al.*, 1987; Appenzeller and Davies, 1992; Appenzeller *et al.*, 1996; Cooper *et al.*, 2004; Pan *et al.*, 2007, 2010]. TST has several commonly occurring transport pathways. The dominant method of TST is slow ascent in the tropics associated with the Brewer-Dobson circulation [Brewer, 1949; Dobson, 1956]. There are also several important mechanisms for TST that take place on shorter time scales. For example, upwelling in the Asian monsoon anticyclone is a topic of active research [Randel *et al.*, 2010, and references therein]. Additionally, TST through isentropic transport of air from the tropical upper troposphere into the midlatitude lowermost stratosphere above the subtropical jet (370–400 K potential temperature range) has received recent attention [e.g., Olsen *et al.*, 2008, 2010; Pan *et al.*, 2009, 2010]. Pan *et al.* [2009] label these exchange events as tropospheric intrusions, parallel to the term “stratospheric intrusions”. They provide diagnostic methods for identifying tropospheric intrusions by

<sup>1</sup>Department of Atmospheric Sciences, Texas A&M University, College Station, Texas, USA.

<sup>2</sup>National Center for Atmospheric Research, Boulder, Colorado, USA.

<sup>3</sup>Division of Marine and Atmospheric Chemistry, Rosenstiel School of Marine and Atmospheric Science, University of Miami, Miami, Florida, USA.

<sup>4</sup>Chemical Sciences Division, NOAA Earth System Research Laboratory, Boulder, Colorado, USA.

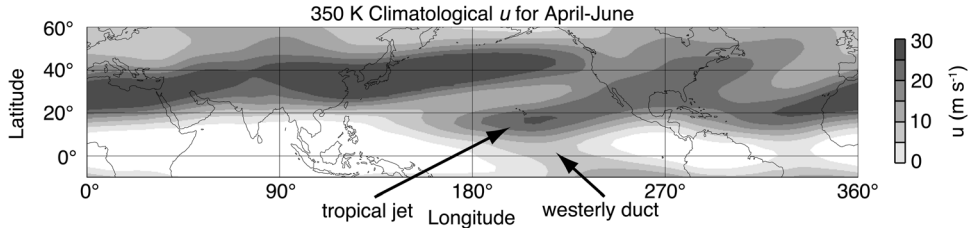


**Figure 1.** Climatological mean zonal wind speed ( $u$ ) on the 350 K potential temperature surface from the NCEP/NCAR reanalysis for April to June 1970–2000. White areas represent regions of climatological mean easterlies.

using static stability and the occurrence of secondary tropopauses. It is well known that tropospheric intrusions have been observed as low-ozone laminae in the stratosphere in many previous studies [e.g., Dobson, 1973]. Irreversibility and frequency of low-ozone laminae has received increasing attention [e.g., Olsen *et al.*, 2010]. At this time extensive research on the detailed chemical composition, frequency and dynamical evolution of these events has not been done.

[4] Tropospheric intrusions have been shown to accompany large-scale Rossby wavebreaking [McIntyre and Palmer, 1983] events in the UTLS in previous studies [e.g., Newman and Schoeberl, 1995; Vaughan and Timmis, 1998; O'Connor *et al.*, 1999; Pan *et al.*, 2009]. As discussed by Pan *et al.* [2009], Rossby wavebreaking has not been studied extensively in the 370–400 K potential temperature range. However, analyses within the works of Postel and Hitchman [2001] and Hitchman and Huesmann [2007] suggest that observations of Rossby wavebreaking on the 350 K isentrope have a positive relationship with the occurrence of Rossby wavebreaking at isentropic surfaces up to the 400 K level, with the exception of Northern Hemisphere spring. The frequency and preferential regions of Rossby wavebreaking illustrated in previous studies suggest that tropospheric intrusions, at least from Rossby wavebreaking, occur commonly in the central Pacific and western Atlantic and have significant seasonal variability [e.g., Postel and Hitchman, 1999, 2001; Hitchman and Huesmann, 2007]. The frequency of Rossby wavebreaking at 350 K has been shown to peak in late spring into summer.

[5] Another possible source for tropospheric intrusions is through Rossby wavebreaking in the so-called “westerly ducts” where mean westerly winds occur in the tropics. Climatological mean westerlies are found in the tropical upper troposphere in two regions of the Northern Hemisphere, predominantly in Northern Hemisphere winter and spring. The southernmost jet is found in the east Pacific between  $\sim 180^\circ$  and  $225^\circ$  longitude and centered at  $\sim 15^\circ\text{N}$  latitude. The second is found over the tropical Atlantic Ocean and centered at  $\sim 20^\circ\text{N}$  latitude. Figure 1 shows the climatological mean zonal wind speed on the 350 K isentropic surface for the tropics and Northern Hemisphere midlatitudes for April–June 1970–2000 from the National Centers for Environmental Prediction (NCEP)/National Center for Atmospheric Research (NCAR) Reanalysis [Kalnay *et al.*, 1996]. The 350 K isentropic surface is often at the core of the subtropical jet and tropical westerly ducts. These westerly ducts are favorable for cross-equatorial propagation of Rossby waves, while easterly winds, which occur throughout most of the tropics, inhibit propagation

[e.g., Webster and Holton, 1982]. The westerly ducts also have a strong association with the El Niño–Southern Oscillation (ENSO). In particular, the Pacific westerly duct is considerably stronger during the ENSO cold phase (or La Niña) and equatorward Rossby wave propagation is increased [Matthews and Kiladis, 1999]. Horinouchi *et al.* [2000] show that within these ducts Rossby wavebreaking creates distinct transport routes for tropical air near the tropopause into the midlatitude lower stratosphere, particularly during the winter season. Waugh and Polvani [2000] further associate intrusions of midlatitude air into the tropics, which are often accompanied by tropospheric intrusions, with the strength of the westerly ducts and ENSO phase. Although this method of transport also involves Rossby wavebreaking, equatorward propagating waves breaking in the westerly ducts are responsible for transport in this case.

[6] In this study, we analyze tropospheric intrusions sampled during the Stratosphere-Troposphere Analyses of Regional Transport 2008 (START08) experiment [Pan *et al.*, 2010]. One goal is to study the transport mechanisms associated with tropospheric intrusions in further detail. In our analysis, we show the dynamical evolution of each event by using high-resolution meteorological analyses from the operational NCEP Global Forecast System (GFS) model. We also use back trajectories to show the source region and transport pathway of each air mass and its relationship to the local meteorological and dynamical field. Another goal of this study is to characterize the chemical properties of the observed intrusions. We use trace constituents with various sources to relate the observed atmospheric composition to the large-scale dynamical fields. Also, by using a simple box model and a selection of gases with tropospheric sources and varying lifetime, we provide an estimate of the mixing time scale for the observed tropospheric intrusion events. A short global analysis of tropospheric intrusions in the 370–400 K potential temperature range during the START08 experiment period is also given.

## 2. Data

### 2.1. START08 Data

[7] In April to June 2008, the START08 project used the National Science Foundation (NSF)–NCAR Gulfstream V (GV) aircraft to investigate trace gas distributions for a variety of meteorological situations. The focus was on tropospheric and stratospheric intrusions, but research flights also targeted gravity wave events and convection. For START08 the GV payload was designed to measure in situ atmospheric trace species in the UTLS and to study their

**Table 1.** AWAS Trace Constituents Used in the Analysis, Their Lifetimes and Destruction (Loss) Processes Considered, and Estimates of Measurement Precision and Uncertainty<sup>a</sup>

Name	Formula	$\tau_t$ (weeks)	$\tau_s$ (weeks)	Loss	Precision	Uncertainty (%)	Absolute Error (%)
3 Pentyl Nitrate	C <sub>5</sub> H <sub>11</sub> ONO <sub>2</sub>	1	<1	OH + hν	0.1 ppt	±5	10
2 Butyl Nitrate	C <sub>4</sub> H <sub>9</sub> ONO <sub>2</sub>	1	1	OH + hν	0.1 ppt	±5	10
Isobutane	i-C <sub>4</sub> H <sub>10</sub>	1	1	OH + Cl	1 ppt	±5	10
Benzene	C <sub>6</sub> H <sub>6</sub>	2	2	OH + Cl	2 ppt	±5	10
Ethyne	C <sub>2</sub> H <sub>2</sub>	3	4	OH + Cl	2 ppt	±5	10
Methyl Nitrate	CH <sub>3</sub> ONO <sub>2</sub>	4	5–7	hν	0.2 ppt	±5	10
Bromoform	CHBr <sub>3</sub>	5	4–6	hν	0.1 ppt	±10	15
Carbon Monoxide	CO	8	12	OH	5 ppb	±5	10
Ethane	C <sub>2</sub> H <sub>6</sub>	10	15	OH + Cl	2 ppt	±3	5
Methylene Chloride	CH <sub>2</sub> Cl <sub>2</sub>	15	42	OH + Cl	0.5 ppt	±5	10
Chloroform	CHCl <sub>3</sub>	20	45	OH + Cl	0.5 ppt	±5	10

<sup>a</sup>The tropospheric and stratospheric photochemical lifetimes are given by  $\tau_t$  and  $\tau_s$ , respectively. Lifetimes are given using Jet Propulsion Laboratory (JPL) recommendations for reaction rates [Sander *et al.*, 2006]. We use  $[OH] = 10^6$  molecules cm<sup>-3</sup>,  $[Cl] = 10^3$  molecules cm<sup>-3</sup> and  $T = 223$  K when approximating stratospheric lifetimes and  $T = 253$  K for tropospheric lifetimes. Absolute error is applied in addition to measurement uncertainty when values get near the limits of detection.

relationship to the observed atmospheric dynamics. The GV aircraft flew 18 flights during the project and sampled strong tropospheric intrusions during two flights: Research Flights 1 and 14 (RF01 and RF14). Additionally, during several flights the aircraft encountered air with tropospheric characteristics in the extratropical lower stratosphere that were not part of tropospheric intrusions observed in the model analyses within a week prior to the observation time.

[8] The START08 flights reached from the Gulf of Mexico to Canada (~25° to 65°N) and from ~120° to 85°W while reaching a maximum altitude of ~14.3 km. A description of the instrument payload can be found in the work of Pan *et al.* [2010]. Many of the parameters measured by instruments on the GV are sampled at 1 Hz, although some trace gas instruments measured less frequently, such as the Advanced Whole Air Sampler (AWAS). The spatial resolution of the 1 Hz data is about 200 m at standard cruise speed.

[9] In our analysis we use selected trace constituents that are useful for diagnosis of large-scale transport. These include ozone (O<sub>3</sub>), carbon monoxide (CO), and several additional trace species with anthropogenic and/or natural sources at the surface. Ozone data are from the National Oceanic and Atmospheric Administration (NOAA) dual-beam ultraviolet (UV) absorption ozone photometer [Proffitt and McLaughlin, 1983]. The NOAA ozone instrument has a precision of 0.6 ppbv and an accuracy of 3%. Carbon monoxide data are from the NCAR Research Aviation Facility (RAF) vacuum UV resonance fluorescence instrument (similar to that given by Gerbig *et al.* [1999]). The RAF carbon monoxide instrument has a precision of 2 ppbv and an accuracy of 5%. For the remaining constituents, we use measurements from the AWAS instrument. The AWAS instrument captures up to 60 samples per flight in stainless-steel canisters, with each canister pressurized to ~3 atmospheres. The time required for AWAS to collect a sample is between ~10 and 40 s, depending on altitude. Samples are analyzed following each flight by using gas chromatography and mass spectrometry to determine the mixing ratio of a large number of trace species. A list of the AWAS trace gases used in our analysis, their approximate lifetimes, and estimates of precision and accuracy is given in Table 1.

## 2.2. GFS Data

[10] For dynamical analysis and trajectory calculations, we use the gridded analyses produced by the NCEP Global Data Assimilation System (GDAS) for the high-resolution Global Forecast System (GFS) spectral model. The GFS analyses are assimilated on a Gaussian grid with a longitude-latitude resolution of 0.3125° × ~0.3125° (~35 km) and 64 hybrid sigma-pressure levels in the vertical. In the UTLS the vertical resolution is typically ~500–1000 m. Analyses are provided daily at 00, 06, 12, and 18 UTC on a 47-level pressure grid. For comparison with in situ observations from START08, the GFS analyses are linearly interpolated in space and time to each flight track.

## 3. Methods

[11] Trajectory analysis of the observed tropospheric intrusions follows the methods given by Bowman *et al.* [2007]. In this study higher-resolution, three-dimensional GFS analysis wind fields are used with the TRAJ3D trajectory model of Bowman [1993] and Bowman and Carrie [2002]. The trajectories for this analysis are computed with 48 time steps per day.

[12] We use a simple box model to help understand the evolution of the mixing ratios of trace species in the tropospheric intrusions observed during START08. The goal of this exercise is to develop some quantitative insight into the relative importance of the various processes that affect the composition of the intrusion. In particular, we are interested in estimating the time scale for mixing of these air masses with the surrounding stratospheric air. The trace species of interest have natural or anthropogenic sources in the lower troposphere or at the surface. This model is similar in concept to previous studies that estimated mixing time scales for entrainment of midlatitude air into the tropical lower stratosphere, although in this case we apply the model to individual intrusions, rather than the climatological effect of multiple transport events [e.g., Minschwaner *et al.*, 1996; Volk *et al.*, 1996; Flocke *et al.*, 1999].

[13] We model the evolution of the composition of an air parcel that originates in the tropical upper troposphere or lower stratosphere and moves into the extratropical lower stratosphere. The mixing ratios of the species of interest,

which have no sources in the UTLS, change due to photochemical losses and in-mixing of stratospheric background air as the intruding air masses move from the tropics into the extratropics. The background stratospheric air normally has a lower mixing ratio than the relatively young air in the intrusion. We model the change in mixing ratio of a given species as

$$\frac{d\chi}{dt} = -\frac{\chi}{\tau_s} + \frac{\chi_s - \chi}{\tau_m} \quad (1)$$

where  $\chi$  is the mixing ratio of the species of interest in the intrusion,  $\chi_s$  is its background stratospheric mixing ratio,  $\tau_s$  is its chemical lifetime in the lower stratosphere (known from experiment), and  $\tau_m$  is the time scale for mixing of background stratospheric air into the intrusion. The second term on the r.h.s. of (1) represents the dilution of the intruding air mass by background stratospheric air. The initial mixing ratio in the tropical upper troposphere and lower stratosphere at  $t = 0$  is  $\chi(0) = \chi_{TTL}$ .

[14] The general solution to (1) is

$$\chi(t_s) = \chi_{TTL} e^{-(\frac{1}{\tau_s} + \frac{1}{\tau_m})t_s} + \frac{\chi_s}{1 + \frac{\tau_m}{\tau_s}} \left(1 - e^{-(\frac{1}{\tau_s} + \frac{1}{\tau_m})t_s}\right) \quad (2)$$

The mixing ratios inside and outside of the intruding air mass,  $\chi(t_s)$  and  $\chi_s$ , are obtained from in situ measurements by the GV aircraft as it flew through the intrusions and the surrounding stratospheric air. The time since the intruding air mass left the tropical upper troposphere,  $t_s$ , is estimated from back trajectories of parcels in the core of the intrusion.

[15] During START08 the GV measured trace gas mixing ratios in the extratropical troposphere, but not in the tropical upper troposphere where the intrusion started. Therefore, we model  $\chi_{TTL}$  as

$$\chi_{TTL} = \chi_t e^{-\frac{1}{\tau_t} t} \quad (3)$$

where  $\chi_t$  is the average extratropical tropospheric mixing ratio (measured by the GV),  $\tau_t$  is its chemical lifetime in the troposphere, and  $t_t$  is the transit time to the tropical upper troposphere. This assumption for  $\chi_{TTL}$  is appropriate for atmospheric constituents that are emitted in midlatitudes and transported to the tropical upper troposphere. It may be inappropriate for species with primary sources that are oceanic and/or tropical (e.g., bromoform and methyl nitrate). Modeling studies suggest, however, that concentrations of these species over the tropical Pacific and Continental United States may be comparable [e.g., Warwick *et al.*, 2006].

[16] The complete solution is then

$$\frac{\chi(t_s)}{\chi_t} = \left(e^{-\frac{1}{\tau_t} t_t}\right) e^{-(\frac{1}{\tau_s} + \frac{1}{\tau_m})t_s} + \frac{\chi_s}{\chi_t \left(\frac{\tau_m}{\tau_s} + 1\right)} \left(1 - e^{-(\frac{1}{\tau_s} + \frac{1}{\tau_m})t_s}\right) \quad (4)$$

which is written here in terms of the ratio of the mixing ratio of the trace gas remaining in the air mass to its initial mixing ratio in the midlatitude troposphere. In this system,  $\chi(t_s)$ ,  $\chi_t$ ,  $\chi_s$ ,  $\tau_t$ ,  $\tau_s$ , and  $t_s$  are known. The mixing time  $\tau_m$  and tropospheric transit time  $t_t$  are unknown. We estimate  $\tau_m$  and  $t_t$  by computing  $\chi(t_s)/\chi_t$  for multiple species and fitting a curve of the form in (4) as a function of chemical lifetime  $\tau_s$

and  $\tau_t$ . We use the nonlinear curve-fitting routine MPFIT in IDL to find  $\tau_m$  and  $t_t$  [Markwardt, 2009]. We also estimate the sensitivity of  $\tau_m$  to uncertainties in  $t_t$ .

[17] For plotting purposes only, in order to display the fit of the box model as a function of a single parameter, we assume a simple relationship between the tropospheric and stratospheric lifetimes. The Arrhenius equation represents the temperature dependence of the rate constant,  $k$ , of a chemical reaction as

$$k = A e^{-\frac{E_a}{RT}} \quad (5)$$

where  $A$  is the preexponential factor,  $E_a$  is the activation energy,  $R$  is the gas constant, and  $T$  is temperature. The lifetime,  $\tau$ , of a given compound is then related to the rate constant  $k$  by  $\tau = 1/(k[C])$ , where  $[C]$  is the concentration of the reactant (e.g., oxidation by OH). For a single reaction, the tropospheric and stratospheric lifetimes can then be related using the relationship between  $\tau$ ,  $k$ , and the Arrhenius equation by

$$\tau_t = e^{\ln(\tau_s) \frac{T_s}{T_t}} \quad (6)$$

where  $\tau_t$  is the tropospheric lifetime,  $\tau_s$  is the stratospheric lifetime,  $T_s$  is the stratospheric temperature, and  $T_t$  is the tropospheric temperature. For our analysis we use  $T_s = 223$  K and  $T_t = 253$  K. This is a reasonable assumption for species that undergo loss predominantly through oxidation processes but would not apply to species whose losses are dominated by photodissociation.

## 4. Results

### 4.1. Research Flight 1

[18] Research Flight 1 (RF01) took place 18 April 2008 and targeted a large mass of tropospheric air that intruded into the stratosphere ~5–8 days earlier. The intrusion is associated with a large-amplitude Rossby wavebreaking event over the western Pacific that occurred from 11 to 16 April. Figure 2 shows potential vorticity (PV) on the 380 K isentropic surface from the GFS analysis at 24 h intervals, illustrating the evolution of the tropospheric intrusion. In Figure 2 the division between red and blue colors is located at 6 pvu, which is representative of the boundary between tropical upper troposphere air and midlatitude lower-stratosphere air at 380 K during this time period. On 11 April the incipient intrusion can be seen just east of Japan (Figure 2a). The intrusion becomes more deformed and stretches farther north until it breaks off from the tropical reservoir around 15 April (Figure 2e). This evolution is consistent with the characteristics of a blocking anticyclone [e.g., Hoskins *et al.*, 1985].

[19] Figure 3a shows the 380 K PV field at 18 UTC on 18 April and the flight track taken by the GV aircraft. To focus on the core of the intrusion, which has the lowest PV values, in Figure 3a the red-blue division is located at 4 pvu. Figure 3b shows the flight track and PV estimated from a 5 day reverse domain filling (RDF) back-trajectory calculation from the analysis time in Figure 3a [Sutton *et al.*, 1994]. The similarity of the analyzed PV and the RDF calculation indicates that the PV in the intrusion was largely

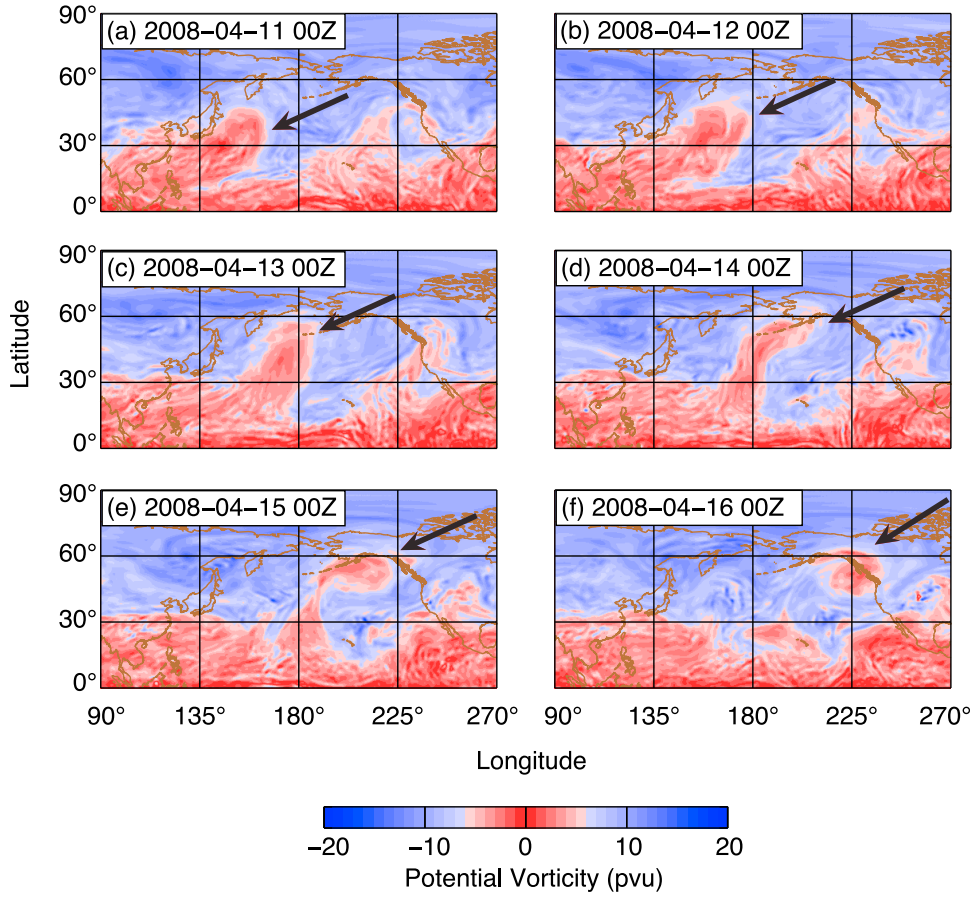


**Figure 2.** Evolution of the tropospheric intrusion event sampled during research flight 1 (RF01). The red colors represent  $|PV| < 6$  pvu on the 380 K isentropic surface from high-resolution GFS analyses. Black arrows identify the intruding air mass.

conserved between the time it intruded into the stratosphere and when it was sampled by the GV.

[20] Figure 4 shows atmospheric parameters from the GFS analysis along a curtain that follows the GV flight track. The intrusion can be seen as air near the 380 K level with lower static stability (lighter colors) and lower values of PV (2–4 pvu), which lies ~3 km above the tropopause. This intrusion of low-stability air may contribute to the stratospheric stability minimum often found above the tropopause inversion layer (TIL), which is defined as the stability maximum within 2–3 km above the tropopause [e.g., Birner et al., 2002; Birner, 2006, 2010; Randel et al., 2007a]. The tropospheric intrusion was sampled multiple times during the first half of the flight along the flight segments labeled 1, 2, and 3. Another stability minimum is observed in the second half of the flight (~1945–2045 UTC), but this is related to a strong cyclone over the central United States, not a tropospheric intrusion [e.g., Bethan et al., 1996; Wirth, 2003; Randel et al., 2007b; Homeyer et al., 2010]. The flight segment labeled 4 sampled air outside the intrusion in the background stratosphere near the 380 K isentropic surface. These four segments are also labeled along the flight track in Figure 3a.

[21] For a different view of the evolution of the intrusion, we examine back trajectories of air parcels from the core of the intrusion. Figure 5, left, shows maps of the locations of

~200 parcels that have  $|PV| < 4$  pvu at both the analysis time for RF01 and 15 days earlier. Figure 5, right, shows vertical sections through the group of parcels. The locations of the vertical sections were chosen subjectively and are shown by the thick black line on each map. The parcels colored red in Figure 5 are those located within  $1^{\circ}$  of the vertical section at each analysis time. Parcels located more than  $1^{\circ}$  from each vertical section are shown on the maps in blue, but are omitted from the vertical section plots for clarity. Because of this selection criterion, the particular parcels colored red and blue are different at each time. In the atmospheric sections, the tropopause altitudes (orange) are calculated by applying the WMO tropopause algorithm to the GFS pressure grid [World Meteorological Organization, 1957]. These tropopause altitudes are consistent with the GFS model output tropopause except in cases of misidentification by the model algorithm near the subtropical jet [Homeyer et al., 2010]. All other variables are from the GFS analysis. On 11 April (Figure 5a), 8 days before the intrusion was sampled, back trajectories show that the parcels are predominantly in a filament in the tropical upper troposphere that stretches westward from the western Pacific where the Rossby wavebreaking event is beginning (see Figure 2). A few parcels are located above the tropopause. On 12 April (Figure 5b), 24 h later, the air mass has moved north into the region of the tropopause break, identified by

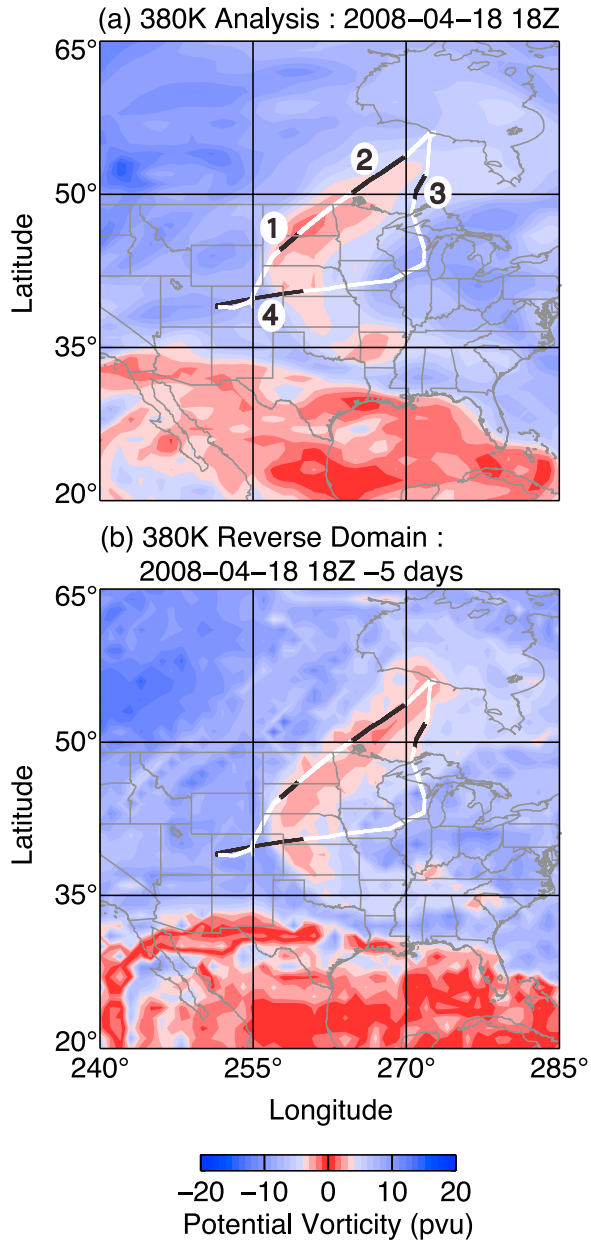


**Figure 3.** Maps for the 380 K isentropic surface showing the flight track taken during research flight 1 (RF01) with (a) analysis PV field for 18 April 2008 at 1800 UTC and (b) 5 day reverse domain PV from the analysis time in Figure 3a. The red colors represent  $|PV| < 4$  ppu from high-resolution GFS analyses. The black portions of the flight track correspond to the horizontal segments labeled in Figure 4. The flight direction is from Colorado to Hudson Bay to southeast Wisconsin to Colorado.

the overlapping (double) tropical and extratropical tropopause, along the edge of the subtropical jet stream [e.g., Palmén, 1948; Danielsen, 1959; Randel et al., 2007a]. By 13 April (Figure 5c) the air mass has moved through the break and into the midlatitude lower stratosphere, where it remains until observed on 18 April. The air mass reaches its highest latitude in the midlatitude lower stratosphere on 15 April (Figure 5d) and then moves east and somewhat south.

At the time the aircraft sampled the tropospheric intrusion, trajectory calculations show that it was completely separated from its tropical source by a strong subtropical jet and the air had been in the lower stratosphere for  $\sim 7$  days.

[22] Observations of long-lived trace species made by the GV provide additional insight into the evolution of the intrusion. Figure 6a is a scatterplot of all O<sub>3</sub>-CO observations during the flight. The relationship between O<sub>3</sub> and CO can be used to identify the stratosphere, troposphere and extratropical transition layer [e.g., Fischer et al., 2000; Hoor et al., 2002; Pan et al., 2004]. Observations during the four horizontal flight segments labeled in Figure 4 are colored by PV to illustrate their relationship to the observed dynamics. Air with low PV ( $< 5.5$  ppu, red) has the strongest tropospheric characteristics, with CO mixing ratios of  $\sim 40$ –60 ppbv (double that of the background stratosphere sampled) and O<sub>3</sub> mixing ratios of  $\sim 100$ –200 ppbv. This air is not typical of the free troposphere, which has higher CO, but it has much lower O<sub>3</sub> than typical stratospheric air. In previous studies, the lower bound of the stratospheric branch is  $\sim 200$ –300 ppb O<sub>3</sub> and  $\sim 30$ –40 ppb CO [e.g., Pan et al., 2004]. Although this low-pv air is not characteristic of the free troposphere, it suggests that the primary origin is in the tropical upper troposphere. Annual mean concentrations of CO in the tropical upper troposphere and lower stratosphere (the tropical tropopause layer or TTL) are 80–90 ppbv and  $\sim 40$  ppbv, respectively [e.g., Tuck et al., 1997; Fueglistaler et al., 2009]. Air near the boundary of the intrusion (6 ppu from Figure 2) is shown in black and is also found in the lower half of the stratospheric branch, with significantly higher O<sub>3</sub> and lower CO than the low-PV air. Air with high PV ( $> 6.5$  ppu, blue) represents the normal stratospheric branch of the O<sub>3</sub>-CO scatterplot. This comparison gives chemical evidence of air in the lower stratosphere with significant tropospheric influence and agrees with the observed PV fields. This relationship is in agreement with that illustrated by Pan et al. [2009].

[23] AWAS data are used to estimate the mixing time scale of the observed intrusion by fitting the model described in section 3 to the measurements. The trajectories for RF01 give an approximate stratospheric transit time  $t_s$  of 1 week. Figure 7a shows the ratio of mean trace gas concentrations in the intrusion to mean tropospheric concentrations for several species,  $\chi(t_s)/\chi_t$ , as a function of stratospheric lifetime  $\tau_s$  for RF01 (black dots). A list of the trace species used is given in Table 1. The values of the model fitted to these ratios by simultaneously varying the two unknown parameters  $t_t$  (the tropospheric transit time) and  $\tau_m$  (the mixing time) are shown by black diamonds. The solid line is the model fit following our assumed relationship between stratospheric and tropospheric lifetimes using the Arrhenius equation (see section 3). Table 2 gives the number of observations used in this analysis and the fitted parameters. For RF01, there are 9 AWAS samples in the intrusion and 8 in the troposphere. The values for  $t_t$  and  $\tau_m$  given by the fit are 0.38 weeks and 0.73 weeks, respectively. The fit is not sensitive to the value of  $t_t$ . If  $t_t$  is varied by  $\pm 1$  week (long/short dashed lines in Figure 7a),  $\tau_m$  changes by less than a day (Table 2). This insensitivity arises because the longer-lived species, which have a strong influence on the shape of the curve, do not undergo significant losses between their source regions and the tropical upper tropo-

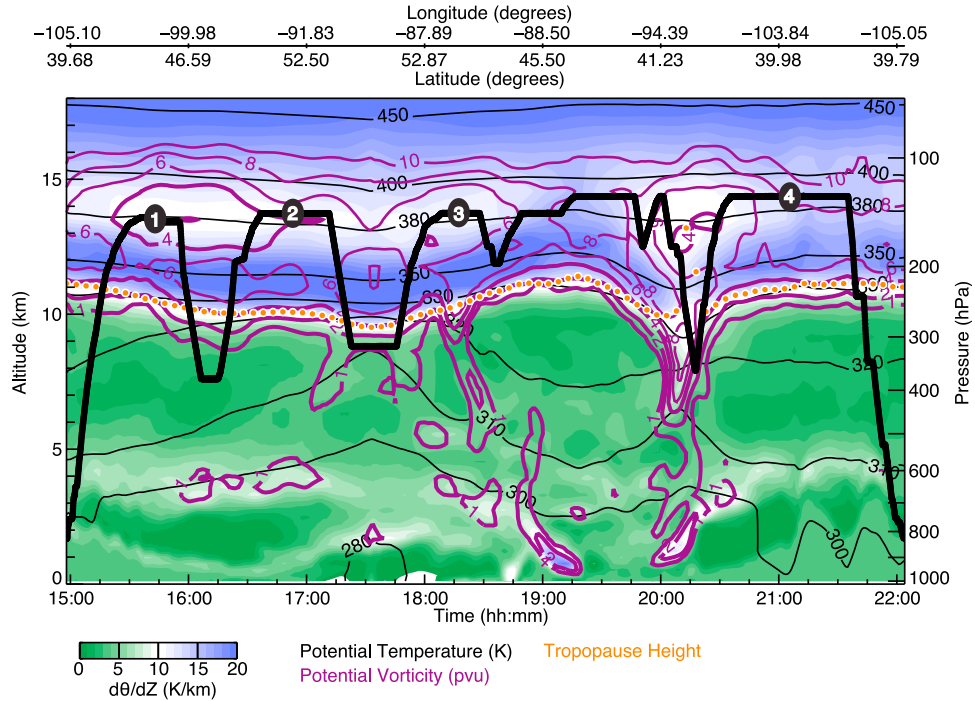


**Figure 4.** A vertical cross section (or curtain) of the atmospheric background for research flight 1 (RF01). All variables are given by high-resolution GFS analyses interpolated to the flight track in space and time. In the curtain, the background is color-filled by the potential temperature lapse rate (or static stability), the orange dots are the NCEP GFS output tropopause height calculated on the model grid, the purple contours are lines of constant potential vorticity, the black contours are potential temperature, and the flight track is the thick black line. Horizontal segments of the flight used for chemical analysis are numbered in white.

sphere. The low sensitivity of  $\tau_m$  to changes in  $t_t$  is a direct result of this relationship and thus the exact value of  $t_t$  is not important for our analysis. On the other hand, varying  $\tau_m$  while holding  $t_t$  fixed causes significant changes to the fit. Increasing or decreasing  $\tau_m$  by a factor of 2 gives the gray envelope in Figure 7a. This indicates that the data constrain  $\tau_m$  well for RF01.

#### 4.2. Research Flight 14

[24] Research Flight 14 (RF14) took place 18 June 2008 and targeted a mass of tropospheric air that intruded into the stratosphere ~4–6 days prior. Unlike RF01, the tropospheric intrusion sampled during RF14 is associated with a slow northward migrating jet in the tropical east Pacific. As discussed briefly in section 1, a persistent westerly jet is observed in this region, particularly during Northern Hemisphere winter and spring. Rossby waves propagate equatorward in the westerlies and break, providing a transport route to midlatitudes. As the jet migrates north, air in the tropical upper troposphere and lower stratosphere above and north of the jet is transported across the tropopause into the midlatitude stratosphere. Figure 8 shows PV on the 390 K isentropic surface from the GFS analysis at 48 h intervals, illustrating the evolution of the observed intrusion. In Figure 8, the division between red and blue colors is located at 4 pvu, which is representative of the boundary between tropical upper troposphere air and midlatitude lower-stratosphere air at 390 K during this time period. It should be noted that the 390 K isentropic surface is fre-

quently very near or above the tropopause in the tropics and some of the low-PV air shown may be in the lower stratosphere [e.g., Seidel *et al.*, 2001]. On 12 June the intrusion can be seen north of Hawaii between 200° and 225° longitude (Figure 8a). Two days later on 14 June the air mass moves farther north and slightly to the east (Figure 8b). By 16 June the air mass separates from the source of tropical air and moves just north of 30°N latitude (Figure 8c). The air mass then moves north and east with the midlatitude westerlies to the northwestern United States by 18 June (Figure 8d, centered near 235° longitude and 50°N latitude).

[25] Following our methods in section 4.1 for RF01, we select horizontal flight segments during RF14 that sampled intrusion air and the stratospheric background for chemical analysis. The atmospheric parameters along a curtain following the flight track for RF14 (not shown) are comparable to those seen for RF01 (Figure 4). The low static stability and PV fields in this case are centered at about 390 K (~3 km above the tropopause). The GV sampled the tropospheric intrusion during two flight segments. The background stratosphere was not measured at 390 K during the flight, so we use one flight segment near 370 K to represent the background stratosphere.

[26] Figure 9 shows maps of parcel locations and vertical sections for parcels from the core of the intrusion. On 11 June (Figure 9a), nearly 8 days before the intrusion was sampled, back-trajectories show that the parcels are above and north of the tropical westerly jet in the east Pacific and

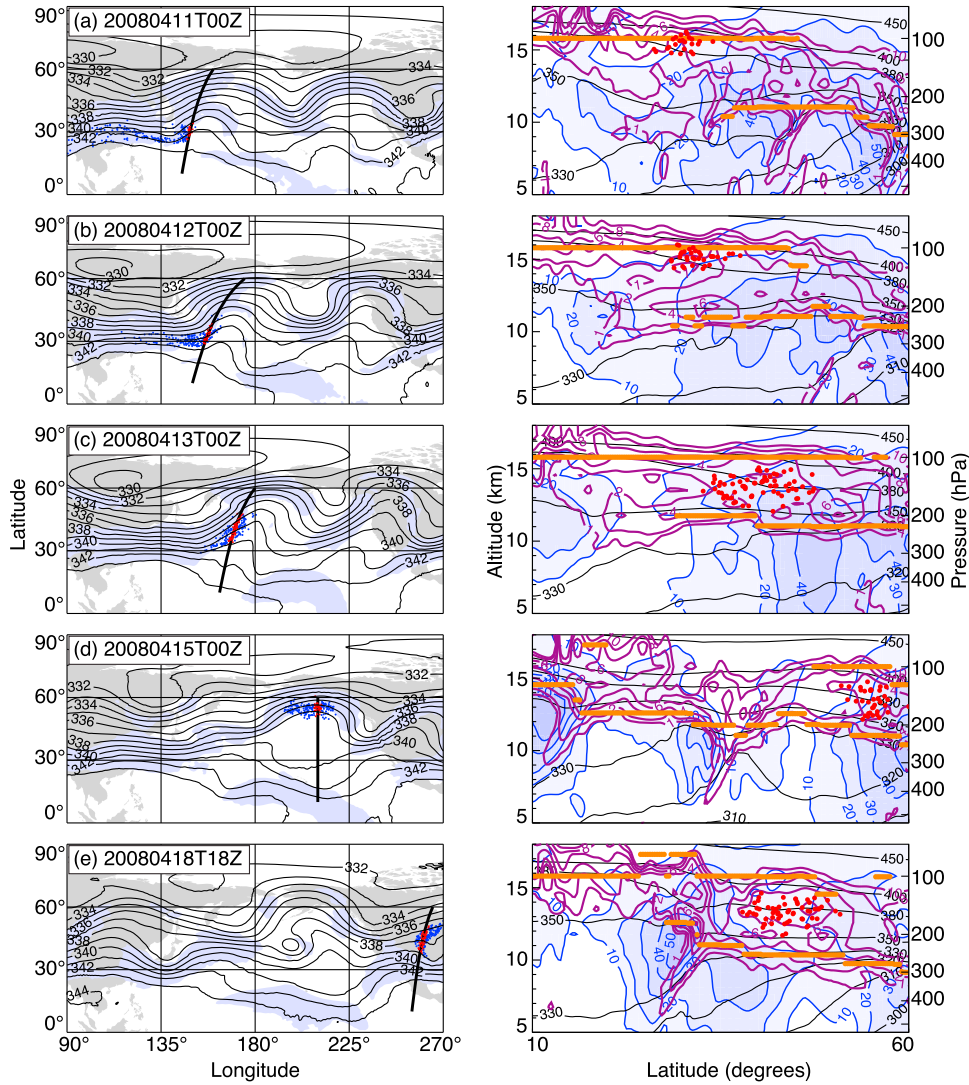


**Figure 5.** (left) Maps showing positions of parcels in the intrusion observed on 18 April. On the maps, wind speeds ( $>30 \text{ m s}^{-1}$ ) at 350 K are shown in light blue, contours of Montgomery stream function (units of  $10^3 \text{ m}^2 \text{ s}^{-2}$ ) are shown in black, trajectory locations are shown as blue and red dots, and the locations of the corresponding vertical section are shown by the thick black lines (great circle arcs). Parcels shown in red on the map correspond to the parcels plotted in red on the vertical section (all parcels within  $1^\circ$  of section). (right) Vertical sections from the GFS analysis of wind speed in  $\text{m s}^{-1}$  (blue colors and contours), potential vorticity in  $\text{pvu}$  (purple), and potential temperature in K (black). The orange lines are tropopause locations calculated using the WMO algorithm.

near the tropopause break in the tropical upper troposphere. By 15 June (Figure 9c) the jet moves north to  $\sim 20^\circ\text{N}$  latitude and the air mass is in the lower stratosphere. Over the next 4 days the air mass moves north and east with the midlatitude westerly flow. During this time the westerlies at mid-latitudes weaken considerably (Figures 9c and 9d), allowing the air mass to be transported north of the subtropical jet where it was sampled with the GV (Figure 9e). At the time the aircraft sampled the tropospheric intrusion, the air had been in the lower stratosphere for  $\sim 5$  days.

[27] Figure 6b is a scatterplot of  $\text{O}_3$  and CO observations during RF14. Observations along flight segments in the intrusion and background stratosphere are again colored by PV (as in Figure 6a). The low-PV air ( $<5.5 \text{ pvu}$ , red) is again at the lower  $\text{O}_3$  bound of the stratospheric branch and

has the highest CO concentrations of the branch. Again, this air is not characteristic of the free troposphere, but the elevated CO concentrations and low  $\text{O}_3$  (compared to the stratospheric background) suggest a significant tropospheric influence.

[28] Results from fitting the box model to the AWAS data are shown in Figure 7b. Trajectories for RF14 give an approximate stratospheric transit time  $t_{\text{strat}}$  of 0.75 weeks for our model. The relationship between the observations and model is similar to the fit for RF01 (Figure 7a). If the tropospheric transit time  $t_t$  is varied  $\pm 1$  week, the mixing time  $\tau_m$  also changes  $\pm 1$  day in this case (see Table 2), again suggesting that  $\tau_m$  has low sensitivity to changes in  $t_t$ . The data also constrain  $\tau_m$  well for RF14. In this case the mixing time given by the model is 0.84 weeks ( $\sim 6$  days), slightly

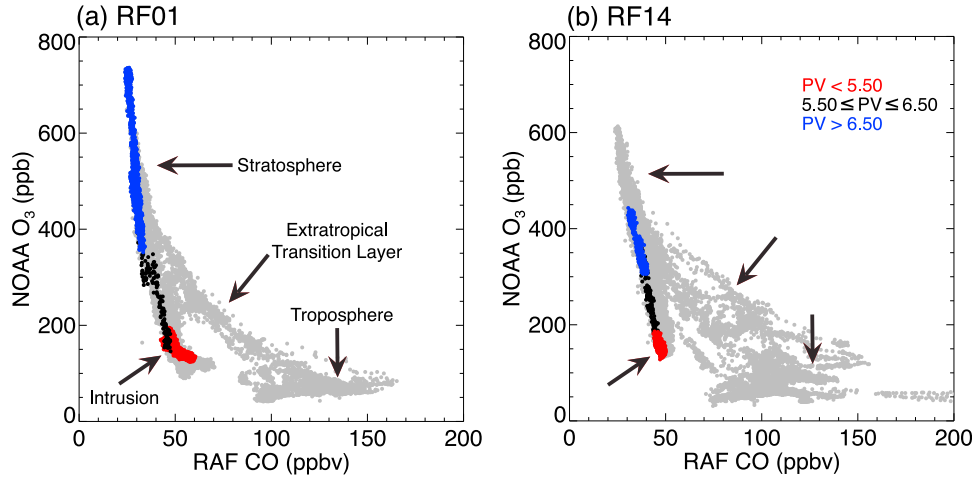


**Figure 6.** Scatterplot of NOAA ozone ( $O_3$ ) and RAF carbon monoxide (CO) for samples taken during (a) RF01 and (b) RF14. All observations are shown in gray. Observations from select horizontal segments (shown for RF01 in Figure 4) are colored by potential vorticity (PV) to illustrate their relationship to the dynamics of the tropospheric intrusion.

longer than in RF01. The variability in  $\tau_m$  for changes in  $t_t$  is slightly, but not significantly, higher for RF14.

#### 4.3. Research Flights 7, 9, and 10

[29] During START08 the GV aircraft observed many small-scale features in the stratosphere with tropospheric chemical characteristics. These features suggest that irreversible transport by tropospheric intrusions is important for lower-stratospheric composition. Three research flights observed air with these characteristics in the 370–400 K potential temperature range at latitudes 10°–15° north of the subtropical jet (RF07, RF09, and RF10). Unlike the large-scale tropospheric intrusions sampled in RF01 and RF14, there are no obvious features with low stability or low PV in the GFS analyses at the locations where these small-scale chemical variations are observed (not shown). All of the

observed features are found ~3–5 km above the tropopause and in regions of  $PV \geq 8$  pvu and static stability  $\geq 14$  K/km for each flight.

[30] Figures 10a, 10b and 10c show measurements of  $O_3$ , CO, and ethyne for RF07, RF09, and RF10, respectively. For each time series, the small-scale features with tropospheric characteristics can be seen in significantly decreased  $O_3$  (300–600 ppb lower than the background stratosphere) and increased CO (10–20 ppbv higher than the background stratosphere). The relevant flight segments are identified by a gray background. The features can also be seen in short-lived tropospheric trace species such as ethyne, which has a lifetime of 3 weeks. In RF07 and RF10 the small-scale features have nearly double the concentration of ethyne compared to the surrounding stratospheric air. The feature observed in RF09 cannot be contrasted with the surrounding

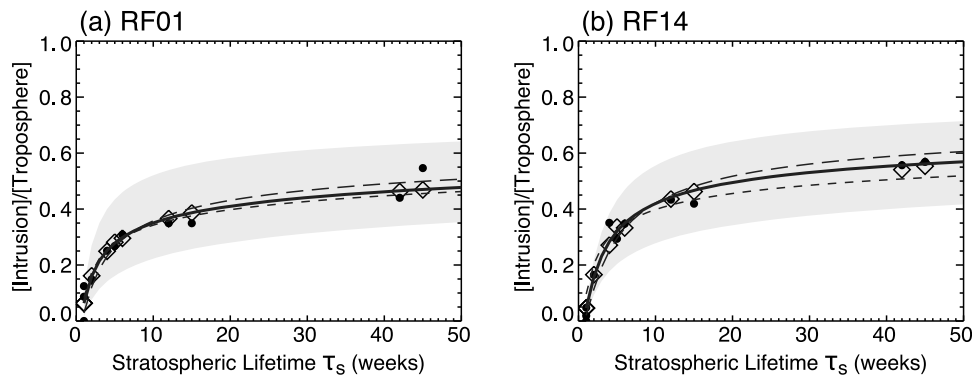


**Figure 7.** The ratio of the mean mixing ratio of trace constituents within the observed intrusion to the mean mixing ratio in the troposphere for (a) RF01 and (b) RF14. The black circles are the aircraft data and the black diamonds are values given using parameters from the fit of the model given in equation (4). The mixing time ( $\tau_m$ ) and tropospheric transit time ( $t_t$ ) of the fit are given in Table 2. The model fit using the lifetime relationship given by the Arrhenius equation is shown in black (solid line). Fits for  $t_t \pm 1$  week are also shown with +1 week long-dashed and -1 week short-dashed. The envelope given by using  $t_t$  from the fit and varying  $\tau_m$  from  $\frac{1}{2}\tau_m$  to  $2\tau_m$  is shown in light gray.

**Table 2.** Number of Observations Used for and Parameters Given by the Box Model Curve Fit

Flight	$n_{int}$	$n_{trop}$	$t_t$ (weeks)	$\tau_m$ (weeks)	$\tau_m((t_t - 1) > 0)$ (weeks)	$\tau_m(t_t + 1)$ (weeks)
RF01	9	8	0.38	0.73	0.67	0.86
RF14	8	21	1.43	0.84	0.65	1.05

air because there is only one AWAS sample during the interval shown. The timeline for RF10 (Figure 10c) ends at the point where the aircraft descended to a lower altitude.

[31] To test whether these small-scale features are produced by stretching and folding by the large-scale resolved flow, we compute 10 day reverse-domain-filled (RDF) maps of equivalent latitude on a high-resolution  $0.1^\circ \times 0.1^\circ$  grid for flights RF07, RF09, and RF10 at the hour nearest in time to when the small-scale features are sampled by the aircraft. Trajectory methods like RDF can often provide detailed information about transport and stirring that Eulerian analyses cannot [e.g., Sutton *et al.*, 1994]. Figures 11a and 11b show RDF maps of equivalent latitude on isentropic surfaces near the level where the air with tropospheric characteristics is observed during flights RF07 and RF10, respectively. The measured CO along the flight track is plotted in green or yellow during times when the aircraft potential temperature is within 5 K of the isentropic surface shown. The narrow gray lines indicate when the aircraft was flying at other altitudes. For both flights elevated levels of CO ( $>30$  ppbv, green) coincide well with filaments of air that has been transported from tropical/subtropical regions, indicated by their low equivalent latitudes of origin ( $\leq 30^\circ$ , red colors). Additionally, background stratospheric levels of CO ( $<30$  ppbv, yellow) are found in air with middle and high equivalent latitudes of origin ( $>30^\circ$ , blue colors).

[32] It is not surprising that the global analyses fail to resolve these rather small-scale features. The RDF analysis shows that they are remnants of intrusions that started more than a week prior to when they were sampled by the GV. Although these features are no longer recognizable in large-scale Eulerian fields, the source air masses are easily identifiable in the in situ measurements from the aircraft and in Lagrangian studies driven by the large-scale winds [e.g., Bowman *et al.*, 2007].

#### 4.4. Global Intrusion Analysis

[33] The following results give a subjective global analysis of tropospheric intrusions in the 370–400 K potential temperature range for the START08 experiment period (April–June 2008) using the GFS analyses. At each model analysis time parcels are initialized on a  $0.5^\circ \times 0.5^\circ \times 10$  K potential temperature grid over the Northern Hemisphere and run backward for 10 days. Using 5 and 10 day RDF maps of equivalent latitude, tropospheric intrusions are manually identified as air masses with equivalent latitude of origin  $\leq 30^\circ$  that are entirely detached from the tropical reservoir and are advected poleward from the reservoir in the period following detachment. During the analysis period 19 tropospheric intrusions can be identified using the aforementioned guidelines. All 19 events are associated with Rossby wavebreaking in one of the forms discussed in section 1. The events vary spatially in size and typically

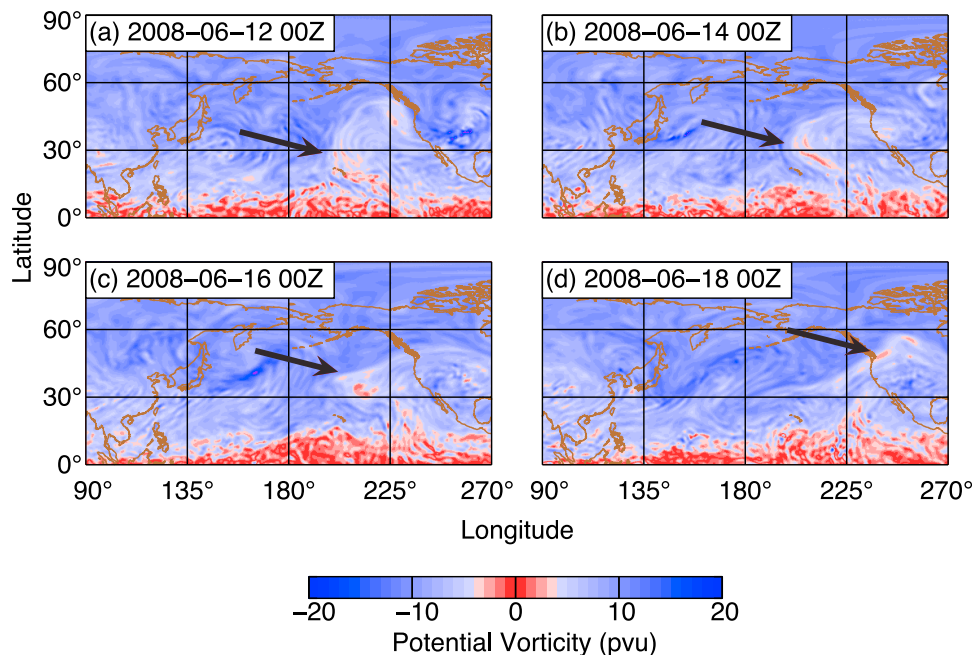


**Figure 8.** Evolution of the tropospheric intrusion event sampled during research flight 14 (RF14). The red colors represent  $|PV| < 4$  pvu on the 390 K isentropic surface from high-resolution GFS analyses. Black arrows identify the intruding air mass.

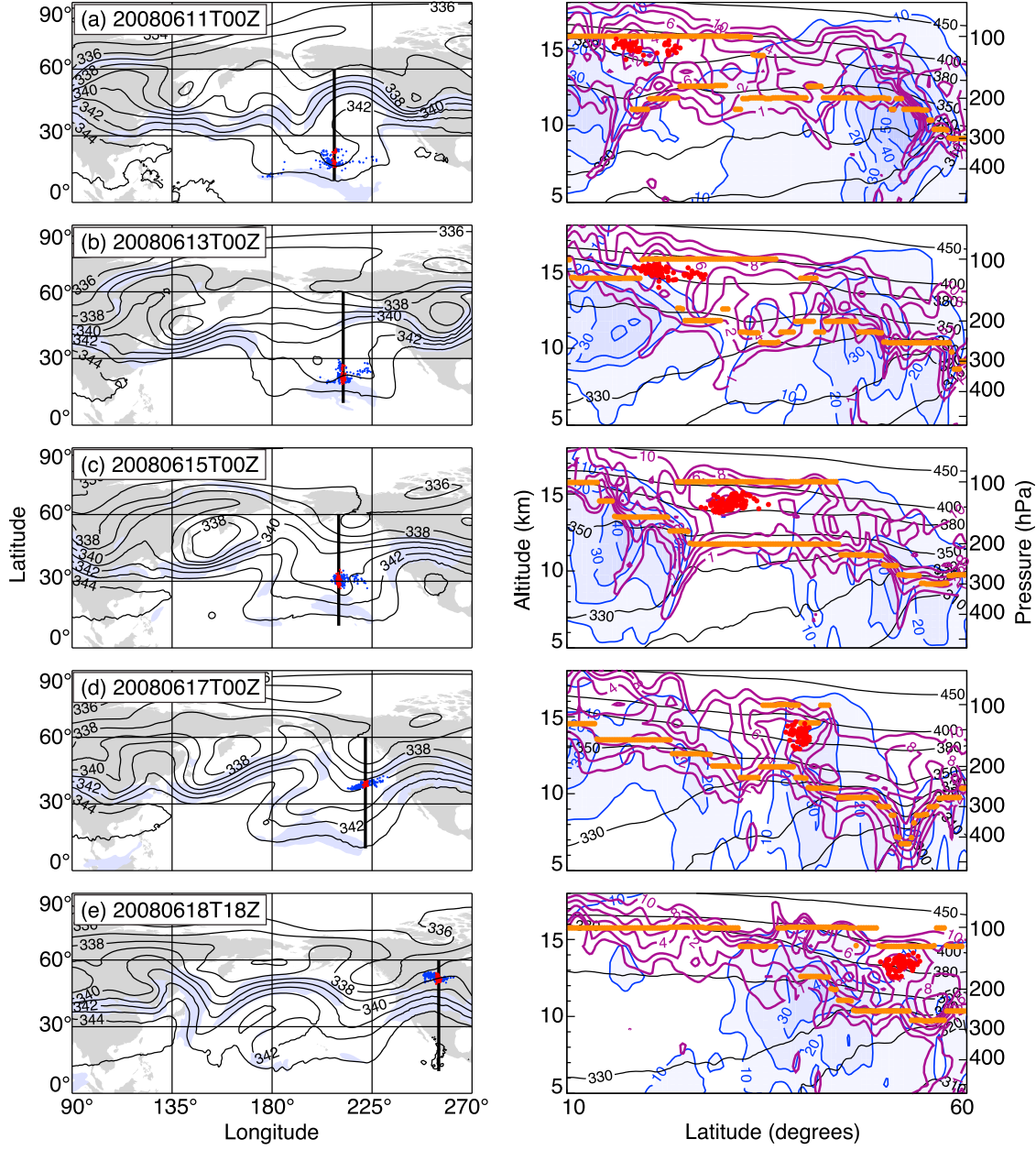


**Figure 9.** As in Figure 5, but for RF14.

intrude and detach within  $\sim 3$  days. The intrusion sampled during RF01 is one of the largest events observed.

[34] Figure 12a is an example that shows 10 day RDF equivalent latitude on the 380 K isentropic surface for an intrusion that resulted from large-amplitude Rossby wave-breaking in the central Pacific. The intrusion air mass and source Rossby wavebreaking event are identified by arrows in the map. Following the analysis time shown, the intrusion and source air masses separate as the source air mass collapses back into the tropical reservoir. Additionally, some of the stratospheric air seen here in the tropics (blue colors in the east Pacific) is mixed in with the tropical reservoir after the breaking event collapses [e.g., Waugh and Polvani, 2000]. We find that the events can be divided into three tropical source regions: the west/central Pacific ( $120^{\circ}$ – $200^{\circ}$  longitude), the east Pacific ( $200^{\circ}$ – $260^{\circ}$  longitude) and the Atlantic

( $280^{\circ}$ – $340^{\circ}$  longitude). The west/central Pacific and Atlantic regions are associated with high-frequency Rossby wave-breaking at 350 K in previous studies (see section 1). The east Pacific region encapsulates the strongest portion of the Pacific westerly duct (see Figure 1) that, when coupled with equatorward Rossby wavebreaking, can provide transport pathways to higher latitudes (see section 1). Figure 12b shows the source regions and the number of intrusion events observed in our analysis. The most active region for tropospheric intrusions during the START08 period is the west/central Pacific, with 11 intrusions observed during the 91 analysis days (a frequency of  $\sim 1$  per week). In the eastern Pacific region, 7 intrusions are observed during the time period (a frequency of  $\sim 1$  every 2 weeks). Only 1 tropospheric intrusion has its source air mass from Rossby wavebreaking over the Atlantic region in our analysis.

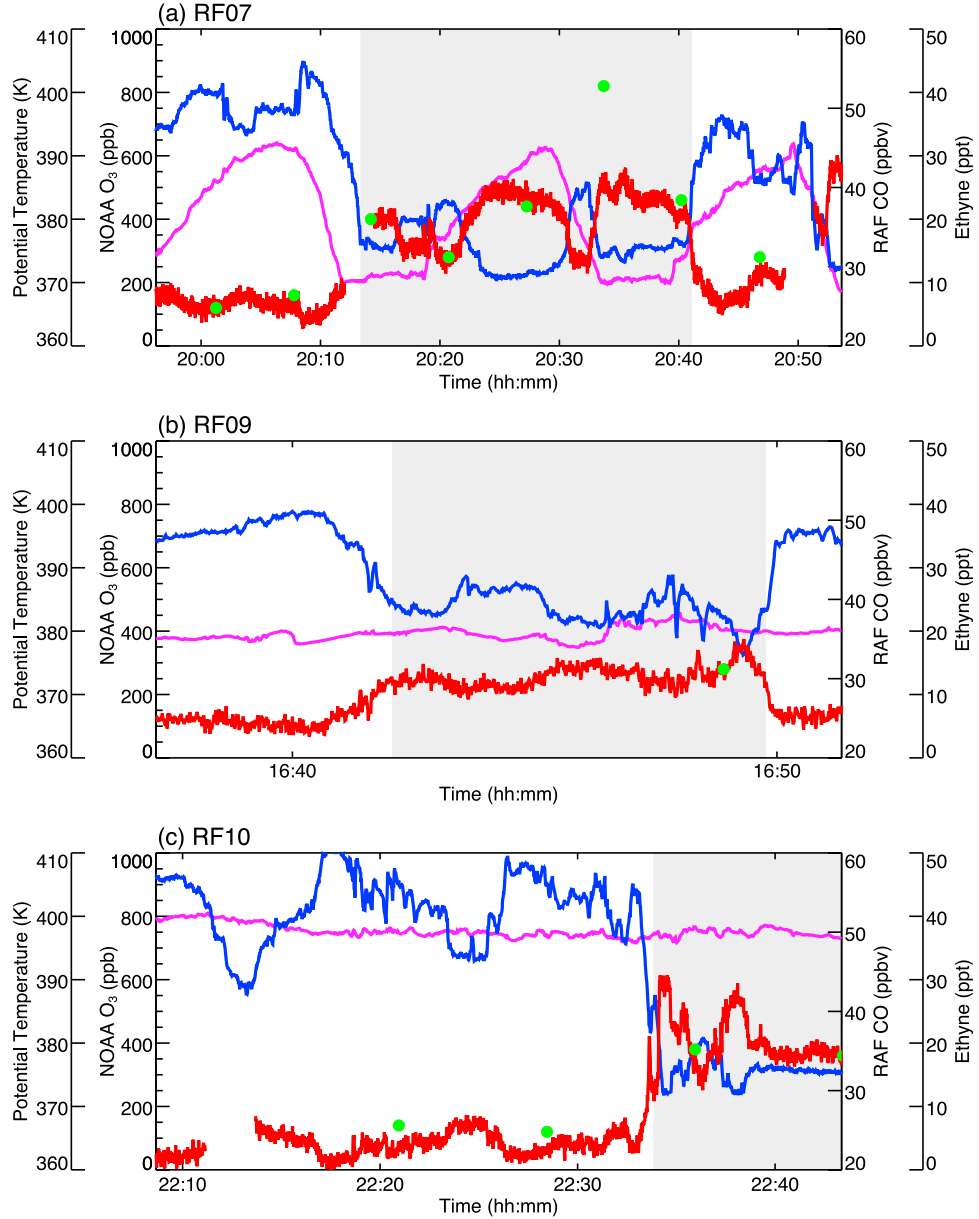


**Figure 10.** Timelines for flight segments where small-scale features of air with tropospheric characteristics are observed for flights (a) RF07, (b) RF09, and (c) RF10. In each plot, the magenta line is potential temperature, the blue line is NOAA ozone ( $O_3$ ), the red line is RAF carbon monoxide (CO), and the green dots are AWAS samples of ethyne ( $C_2H_2$ ). The periods containing air with tropospheric characteristics are identified by a gray background.

[35] Tropospheric intrusion events over the west/central Pacific and east Pacific regions have very different character during the time period. In the west/central Pacific intrusions typically resemble the one sampled by RF01 (see Figure 2). In the east Pacific, the intrusion events are all similar to that in RF14 (see Figure 8), with slow evolution dominated by meridional transport. These different characteristics can be related to the different Rossby wavebreaking regimes discussed in section 1. Rossby wavebreaking along the subtropical jet stream and north of the westerly ducts typically occurs in zonal flow. When Rossby waves propagate equatorward and break within the westerly ducts, however, the zonal component is in the deep tropics and intrusions are

transported primarily in the meridional direction. These evolutionary differences have been classified before by [Peters and Waugh, 1996] as type 1 (tilts downstream, broadens, wraps up anticyclonically) and type 2 (tilts upstream, thins, advected cyclonically) poleward breaking events. It is evident from our analysis that large-amplitude Rossby wavebreaking events are predominantly type 1 and Rossby wavebreaking in the westerly ducts, type 2. It should also be noted that previous studies suggest that the west/central Pacific and Atlantic regions should be comparable in Rossby wavebreaking frequency, at least at 350 K. However, 2008 was predominantly an ENSO cold phase (La Niña) year which

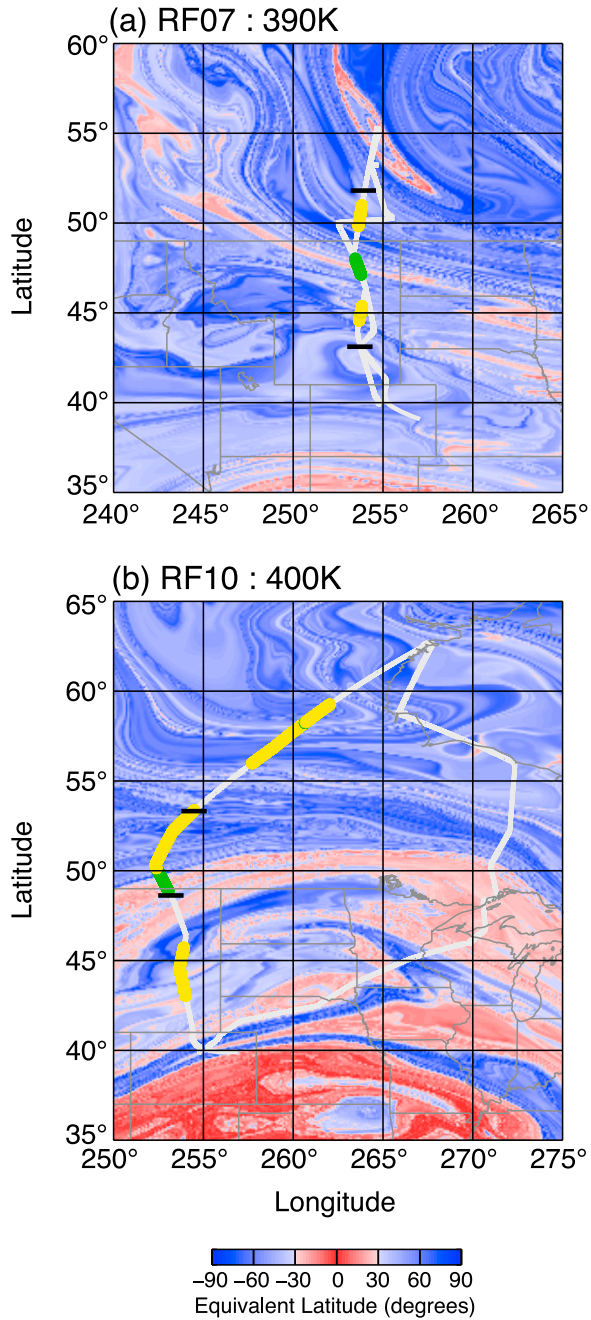


**Figure 11.** Maps of 10 day reverse-domain-filled (RDF) equivalent latitude for (a) RF07 on the 390 K isentropic surface and (b) RF10 on the 400 K isentropic surface. The flight track is shown in gray and colored by carbon monoxide (CO) mixing ratio ( $<30$  ppbv, yellow;  $>30$  ppbv, green) where the aircraft potential temperature is within 5 K of the isentropic surface for each map. Black tick marks on the flight track correspond to the timelines shown in Figure 10.

could explain the observed frequency of tropospheric intrusions in the east Pacific and Atlantic regions.

## 5. Summary and Discussion

[36] Tropospheric intrusions observed during START08 show good correspondence between the observed kinemat-

ics from the NCEP GFS analyses and in situ measurements of trace gases aboard the aircraft. The tropospheric intrusions sampled by the GV aircraft can be traced back to Rossby wavebreaking events. For both RF01 and RF14, intruding air from the tropical upper troposphere was sampled well north of the subtropical jet and several kilometers above the extratropical tropopause. Back trajectories show that transport in these events took place above the subtropical jet and along isentropic surfaces (Figures 5 and 9). The intruding air masses are characterized by low PV, low static stability, and chemical composition more typical of the troposphere.

[37] The mixing time scales of the observed tropospheric intrusions can be estimated by fitting a simple box model (section 3) to trace species with varying lifetimes (Table 1). The model fits for both RF01 and RF14 give a mixing time scale of 5 to 6 days. This mixing time scale is an important parameter to understand when considering this type of transport and mixing in applications such as chemistry-climate model validation (CCMVal) [Eyring et al., 2005].

[38] A global analysis of tropospheric intrusions for April–June 2008 found 19 significant tropospheric intrusions. All but one of the intrusion events had its source over the Tropical Pacific. In our analysis, we found Rossby wavebreaking in the west/central Pacific and east Pacific regions to be common, with a higher frequency of occurrence in the west/central Pacific. Tropospheric intrusions in the west/central Pacific are related to high-frequency large-amplitude Rossby wavebreaking events as discussed in the previous literature [e.g., Postel and Hitchman, 1999, 2001; Hitchman and Huesmann, 2007]. Tropospheric intrusions in the east Pacific region are related to equatorward Rossby wavebreaking in the Pacific westerly duct. The high frequency of tropospheric intrusions in the east Pacific may be due to La Niña conditions present during 2008.

[39] Several filaments of air with tropospheric properties were observed in the 370–400 K potential temperature range during START08. These filaments are seen in the in situ trace gas measurements by the aircraft, but the Eulerian analyses fail to represent these small-scale features. As discussed in section 4.3, it is likely that these air masses were part of larger tropospheric intrusion events more than a week prior to being sampled by the GV aircraft. Therefore, the intrusions have had time to mix further and deform with the large-scale synoptic flow, rendering them indistinguishable in large-scale dynamical and meteorological fields. The air still possesses, however, characteristics that are significantly different than the surrounding background stratosphere (Figure 10). These observations suggest that irreversible transport by tropospheric intrusion events is common, at least during the START08 experiment period (April–June 2008). Further confirmation of a relationship between the filaments and prior tropospheric intrusion events was found by using reverse-domain-filled maps of equivalent latitude (Figure 11). This approach provides a more detailed representation of tropospheric intrusions and their filamentation than the diagnostics given by Pan et al. [2009]. It can also be used for operational forecasts in future aircraft missions.

[40] It is evident from our analysis during the START08 experiment that tropospheric intrusions are a common mechanism of STE. These intrusions can have a significant

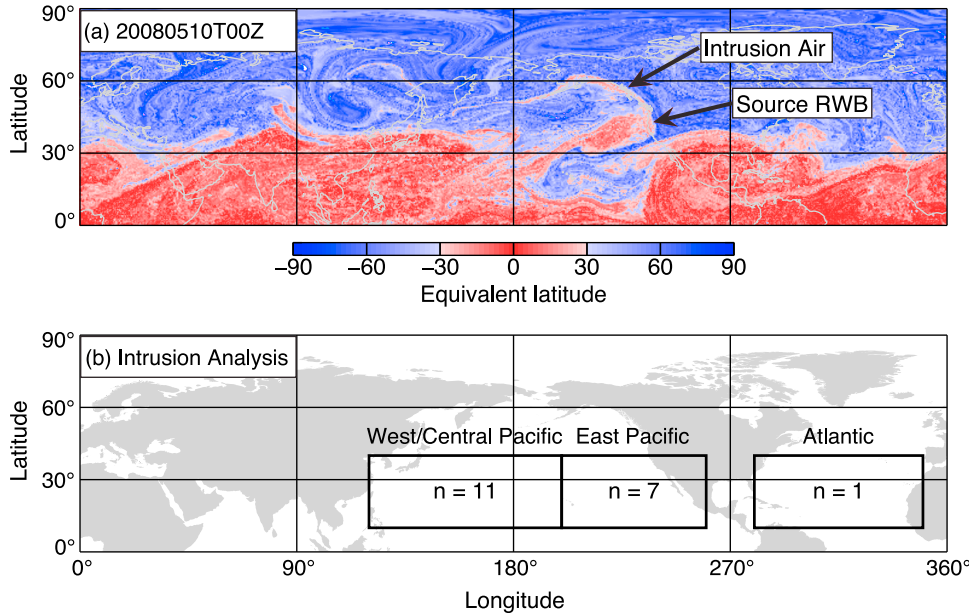


**Figure 12.** Maps of (a) an example 10 day reverse-domain-filled (RDF) equivalent latitude calculation on the 380 K isentropic surface valid 10 May 2008 at 00 UTC used for the global tropospheric intrusion analysis and (b) number of intrusions observed by region for the global analysis.

impact on the composition and distribution of trace species in the middle world. Although tropospheric intrusions can be readily related to large-amplitude Rossby wavebreaking over the Pacific and Atlantic oceans, breaking of equatorward propagating Rossby waves in the westerly ducts appears to play a significant role, which may be more significant during the ENSO cold phase (La Niña).

[41] **Acknowledgments.** We acknowledge the START08 project for access to the aircraft data and motivation for this study. This research was funded by National Science Foundation grants ATM-072225 and AGS-1016191 to Texas A&M University.

## References

- Appenzeller, C., and H. C. Davies (1992), Structure of stratospheric intrusions into the troposphere, *Nature*, **358**, 570–572.
- Appenzeller, C., H. C. Davies, and W. A. Norton (1996), Fragmentation of stratospheric intrusions, *J. Geophys. Res.*, **101**(D1), 1435–1456.
- Bethan, S., G. Vaughan, and S. J. Reid (1996), A comparison of ozone and thermal tropopause heights and the impact of tropopause definition on quantifying the ozone content of the troposphere, *Q. J. R. Meteorol. Soc.*, **122**, 929–944.
- Birner, T. (2006), Fine-scale structure of the extratropical tropopause, *J. Geophys. Res.*, **111**, D04104, doi:10.1029/2005JD006301.
- Birner, T. (2010), Residual circulation and tropopause structure, *J. Atmos. Sci.*, **67**, 2582–2600, doi:10.1175/2010JAS3287.1.
- Birner, T., A. Dörnbrack, and U. Schumann (2002), How sharp is the tropopause at midlatitudes?, *Geophys. Res. Lett.*, **29**(14), 1700, doi:10.1029/2002GL015142.
- Bowman, K. P. (1993), Large-scale isentropic mixing properties of the Antarctic polar vortex from analyzed winds, *J. Geophys. Res.*, **98**(D12), 23,013–23,027.
- Bowman, K. P., and G. D. Carrie (2002), The mean-meridional transport circulation of the troposphere in an idealized GCM, *J. Atmos. Sci.*, **59**, 1502–1514.
- Bowman, K. P., L. L. Pan, T. Campos, and R. Gao (2007), Observations of fine-scale transport structure in the upper troposphere from the High-performance Instrumented Airborne Platform for Environmental Research, *J. Geophys. Res.*, **112**, D18111, doi:10.1029/2007JD008685.
- Brewer, A. W. (1949), Evidence for a world circulation provided by the measurements of helium and water vapour distribution in the stratosphere, *Q. J. R. Meteorol. Soc.*, **75**, 351–363.
- Browell, E. V., E. F. Danielsen, S. Ismail, G. L. Gregory, and S. M. Beck (1987), Tropopause fold structure determined from airborne lidar in situ measurements, *J. Geophys. Res.*, **92**(D2), 2112–2120.
- Cooper, O., et al. (2004), On the life cycle of a stratospheric intrusion and its dispersion into polluted warm conveyor belts, *J. Geophys. Res.*, **109**, D23S09, doi:10.1029/2003JD004006.
- Danielsen, E. F. (1959), The laminar structure of the atmosphere and its relation to the concept of a tropopause, *Arch. Meteorol. Geophys. Bioklimatol., Ser. A*, **11**, 293–332.
- Danielsen, E. F. (1968), Stratospheric-tropospheric exchange based on radioactivity, ozone and potential vorticity, *J. Atmos. Sci.*, **25**, 502–518.
- Dobson, G. M. B. (1956), Origin and distribution of the polyatomic molecules in the atmosphere, *Proc. R. Soc. London*, **236**(1205), 187–193.
- Dobson, G. M. B. (1973), The laminated structure of the ozone in the atmosphere, *Q. J. R. Meteorol. Soc.*, **99**(422), 599–607.
- Eyring, V., et al. (2005), A strategy for process-oriented validation of coupled chemistry-climate models, *Bull. Am. Meteorol. Soc.*, **86**(8), 1117–1133.
- Fischer, H., F. G. Wienhold, P. Hoor, O. Bujok, C. Schiller, P. Siegmund, M. Ambaum, H. A. Scheeren, and J. Lelieveld (2000), Tracer correlations in the northern high latitude lowermost stratosphere: Influence of cross-tropopause mass exchange, *Geophys. Res. Lett.*, **27**(1), 97–100.
- Flocke, F., et al. (1999), An examination of chemistry and transport processes in the tropical lower stratosphere using observations of long-lived and short-lived compounds obtained during STRAT and POLARIS, *J. Geophys. Res.*, **104**(D21), 26,625–26,642.
- Fueglistaler, S., A. E. Dessler, T. J. Dunkerton, I. Folkins, Q. Fu, and P. W. Mote (2009), Tropical tropopause layer, *Rev. Geophys.*, **47**, RG1004, doi:10.1029/2008RG000267.
- Gerbig, C., S. Schmitgen, D. Kley, A. Volz-Thomas, K. Dewey, and D. Haaks (1999), An improved fast-response vacuum-UV resonance fluorescence CO instrument, *J. Geophys. Res.*, **104**(D1), 1699–1704.
- Hitchman, M. H., and A. S. Huesmann (2007), A seasonal climatology of Rossby wave breaking in the 320–2000K layer, *J. Atmos. Sci.*, **64**, 1922–1940.
- Holton, J. R., P. H. Haynes, M. E. McIntyre, A. R. Douglass, and L. Pfister (1995), Stratosphere-troposphere exchange, *Rev. Geophys.*, **33**(4), 403–439.
- Homeyer, C. R., K. P. Bowman, and L. L. Pan (2010), Extratropical tropopause transition layer characteristics from high-resolution sounding data, *J. Geophys. Res.*, **115**, D13108, doi:10.1029/2009JD013664.
- Hoor, P., H. Fischer, L. Lange, J. Lelieveld, and D. Brunner (2002), Seasonal variations of a mixing layer in the lowermost stratosphere as

- identified by the CO-O<sub>3</sub> correlation from in situ measurements, *J. Geophys. Res.*, 107(D5), 4044, doi:10.1029/2000JD000289.
- Horinouchi, T., F. Sassi, and B. A. Boville (2000), Synoptic-scale Rossby waves and the geographic distribution of lateral transport routes between the tropics and extratropics in the lower stratosphere, *J. Geophys. Res.*, 105(D21), 26,579–26,592.
- Hoskins, B. J. (1991), Towards a PV-theta view of the general circulation, *Tellus*, 43, 27–35.
- Hoskins, B. J., M. E. McIntyre, and A. W. Robertson (1985), On the use and significance of isentropic potential vorticity maps, *Q. J. R. Meteorol. Soc.*, 111(470), 877–946.
- Kalnay, E., et al. (1996), The NCEP/NCAR 40-year reanalysis project, *Bull. Am. Meteorol. Soc.*, 77(3), 437–471.
- Markwardt, C. B. (2009), Non-linear least squares fitting in IDL with MPFIT, in *Astronomical Data Analysis Software and Systems (ADASS) XVIII*, Astron. Soc. Pac. Conf. Ser., vol. 411, edited by D. Bohlender, P. Dowler, and D. Durand, pp. 251–254, Astron. Soc. Pac., San Francisco, Calif.
- Matthews, A. J., and G. N. Kiladis (1999), Interactions between ENSO, transient circulation, and tropical convection over the Pacific, *J. Clim.*, 12, 3062–3086.
- McIntyre, M. E., and T. N. Palmer (1983), Breaking planetary waves in the stratosphere, *Nature*, 305(13), 593–600.
- Minschwaner, K., A. E. Dessler, J. W. Elkins, C. M. Volk, D. W. Fahey, M. Loewenstein, J. R. Podolske, A. E. Roche, and K. R. Chan (1996), Bulk properties of isentropic mixing into the tropics in the lower stratosphere, *J. Geophys. Res.*, 101(D5), 9433–9439.
- Newman, P. A., and M. R. Schoeberl (1995), A reinterpretation of the data from the NASA stratosphere-troposphere exchange project, *Geophys. Res. Lett.*, 22(18), 2501–2504.
- O'Connor, F. M., G. Vaughan, and H. De Backer (1999), Observations of subtropical air in the European mid-latitude lower stratosphere, *Q. J. R. Meteorol. Soc.*, 125, 2965–2986.
- Olsen, M. A., A. R. Douglass, P. A. Newman, J. C. Gille, B. Nardi, V. A. Yudin, D. E. Kinnison, and R. Khosravi (2008), HIRDLS observations and simulation of a lower stratospheric intrusion of tropical air to high latitudes, *Geophys. Res. Lett.*, 35, L21813, doi:10.1029/2008GL035514.
- Olsen, M. A., A. R. Douglass, M. R. Schoeberl, J. M. Rodriguez, and Y. Yoshida (2010), Interannual variability of ozone in the winter lower stratosphere and the relationship to laminar and irreversible transport, *J. Geophys. Res.*, 115, D15305, doi:10.1029/2009JD013004.
- Palmén, E. (1948), On the distribution of temperature and wind in the upper westerlies, *J. Meteorol.*, 5, 20–27.
- Pan, L. L., W. J. Randel, B. L. Gary, M. J. Mahoney, and E. J. Hintsa (2004), Definitions and sharpness of the extratropical tropopause: A trace gas perspective, *J. Geophys. Res.*, 109, D23103, doi:10.1029/2004JD004982.
- Pan, L. L., et al. (2007), Chemical behavior of the tropopause observed during the stratosphere-troposphere analyses of regional transport experiment, *J. Geophys. Res.*, 112, D18110, doi:10.1029/2007JD008645.
- Pan, L. L., W. J. Randel, J. C. Gille, W. D. Hall, B. Nardi, S. Massie, V. Yudin, R. Khosravi, P. Konopka, and D. Tarasick (2009), Tropospheric intrusions associated with the secondary tropopause, *J. Geophys. Res.*, 114, D10302, doi:10.1029/2008JD011374.
- Pan, L. L., et al. (2010), The Stratosphere-Troposphere Analyses of Regional Transport 2008 experiment, *Bull. Am. Meteorol. Soc.*, 91, 327–342.
- Peters, D., and D. W. Waugh (1996), Influence of barotropic shear on the poleward advection of upper-tropospheric air, *J. Atmos. Sci.*, 53(21), 3013–3031.
- Postel, G. A., and M. H. Hitchman (1999), A climatology of Rossby wave breaking along the subtropical tropopause, *J. Atmos. Sci.*, 56, 359–373.
- Postel, G. A., and M. H. Hitchman (2001), A case study of Rossby wave breaking along the subtropical tropopause, *Mon. Weather Rev.*, 129, 2555–2569.
- Proffitt, M. H., and R. J. McLaughlin (1983), Fast-response dual-beam UV-absorption ozone photometer suitable for use on stratospheric balloons, *Rev. Sci. Instrum.*, 54(12), 1719–1728.
- Randel, W. J., D. J. Seidel, and L. L. Pan (2007a), Observational characteristics of double tropauses, *J. Geophys. Res.*, 112, D07309, doi:10.1029/2006JD007904.
- Randel, W. J., F. Wu, and P. Forster (2007b), The extratropical tropopause inversion layer: Global observations with GPS data, and a radiative forcing mechanism, *J. Atmos. Sci.*, 64, 4489–4496.
- Randel, W. J., M. Park, L. Emmons, D. Kinnison, P. Bernath, K. A. Walker, C. Boone, and H. Pumphrey (2010), Asian monsoon transport of pollution to the stratosphere, *Science*, 328, 611–613.
- Sander, S. P., et al. (2006), Chemical kinetics and photochemical data for use in atmospheric studies: Evaluation number 15, *Jet Propul. Lab.*, 6(2), 1–77.
- Seidel, D. J., R. J. Ross, J. K. Angell, and G. C. Reid (2001), Climatological characteristics of the tropical tropopause as revealed by radiosondes, *J. Geophys. Res.*, 106(D8), 7857–7878.
- Shapiro, M. A. (1980), Turbulent mixing within tropopause folds as a mechanism for the exchange of chemical constituents between the stratosphere and troposphere, *J. Atmos. Sci.*, 37, 994–1004.
- Stohl, A., H. Wernli, P. James, M. Bourqui, C. Forster, M. A. Liniger, P. Seibert, and M. Sprenger (2003), A new perspective of stratosphere-troposphere exchange, *Bull. Am. Meteorol. Soc.*, 84(11), 1565–1573.
- Sutton, R. T., H. Maclean, R. Swinbank, A. O'Neill, and F. W. Taylor (1994), High-resolution stratospheric tracer fields estimated from satellite observations using Lagrangian trajectory calculations, *J. Atmos. Sci.*, 51(20), 2995–3005.
- Tuck, A. F., et al. (1997), The Brewer-Dobson circulation in the light of high altitude *in situ* aircraft observations, *Q. J. R. Meteorol. Soc.*, 123(537), 1–69.
- Vaughan, G., and C. Timmis (1998), Transport of near-tropopause air into the lower midlatitude stratosphere, *Q. J. R. Meteorol. Soc.*, 124, 1559–1578.
- Volk, C. M., et al. (1996), Quantifying transport between the tropical and mid-latitude lower stratosphere, *Science*, 272(5269), 1763–1768.
- Warwick, N. J., J. A. Pyle, G. D. Carver, X. Yang, N. H. Savage, F. M. O'Connor, and R. A. Cox (2006), Global modeling of biogenic bromocarbons, *J. Geophys. Res.*, 111, D24305, doi:10.1029/2006JD007264.
- Waugh, D. W., and L. M. Polvani (2000), Climatology of intrusions into the tropical upper troposphere, *Geophys. Res. Lett.*, 27(23), 3857–3860.
- Webster, P. J., and J. R. Holton (1982), Cross-equatorial response to middle-latitude forcing in a zonally varying basic state, *J. Atmos. Sci.*, 39, 722–733.
- Wirth, V. (2003), Static stability in the extratropical tropopause region, *J. Atmos. Sci.*, 60, 1395–1409.
- World Meteorological Organization (1957), Meteorology: A three-dimensional science: Second session of the commission for aerology, *World Meteorol. Org. Bull.*, 4, 134–138.

E. L. Atlas, MAC, RSMAS, University of Miami, 4600 Rickenbacker Causeway, Miami, FL 33149, USA. (eatlas@rsmas.miami.edu)

K. P. Bowman and C. R. Homeyer, Department of Atmospheric Sciences, Texas A&M University, 3150 TAMU, College Station, TX 77843-3150, USA. (k-bowman@tamu.edu; chomeyer@tamu.edu)

T. L. Campos, National Center for Atmospheric Research, 1850 Table Mesa Dr., Boulder, CO 80305, USA. (campos@ucar.edu)

R.-S. Gao, Chemical Sciences Division, NOAA ESRL, 325 Broadway, R/CSD6, Boulder, CO 80305, USA. (rushan.gao@noaa.gov)

L. L. Pan, National Center for Atmospheric Research, PO Box 3000, Boulder, CO 80307-3000, USA. (liwen@ucar.edu)